

Kinetic electron emission induced by grazing scattering of slow atoms: Local probe of the Compton profile near the Fermi edge

HP. Winter

Institut für Allgemeine Physik, Vienna University of Technology, Wiedner Hauptstr. 8-10, A-1040 Vienna, Austria

S. Lederer and H. Winter*

Institut für Physik, Humboldt Universität zu Berlin, Newtonstr. 15, D-12489 Berlin-Adlershof, Germany

C. Lemell and J. Burgdörfer

Institute for Theoretical Physics, Vienna University of Technology, Wiedner Hauptstr. 8-10, A-1040 Vienna, Austria

(Received 13 May 2005; published 13 October 2005)

Kinetic electron emission induced by noble gas atoms impinging at low (keV) energies on an Al(111) surface under a grazing angle of incidence is studied by coincident time-of-flight and electron number spectroscopy. We observe small but defined yields for electron emission γ at impact velocities below the “classical” threshold for kinetic emission of quasifree metal electrons. An analysis within the impulse approximation indicates that subthreshold emission may serve as a probe for the local electron momentum distribution (Compton profile) above the topmost layer of metal targets.

DOI: 10.1103/PhysRevB.72.161402

PACS number(s): 79.20.Rf, 61.85.+p, 79.60.Bm

Electron emission induced by heavy particles (ions, atoms) impacting on surfaces has been investigated in considerable detail.¹ Different ejection processes can be distinguished: potential emission (PE) by which the potential energy of the projectile carried into the collision is converted into electronic excitation in the continuum and kinetic emission (KE) by which part of the kinetic energy of the projectile is imparted on target electrons, mostly in binary collision events. For grazing incidence, separation of PE and KE contributions, both present for ionic projectiles, has been achieved.² Investigations of pure KE require the use of neutral atoms in their ground state for which PE is suppressed.

Interest in KE results, in part, from the fact that KE may provide information on both the interaction process and properties of the surface. For example, KE and (electronic) stopping of atomic projectiles are closely interrelated, since both processes comprise excitations of conduction electrons.³ Juaristi *et al.*⁴ found for normal incidence of projectiles that the KE yield, γ_{KE} , is proportional to the stopping power at low energies.³

In this paper we find evidence that KE induced by low-energy neutral atom scattering at grazing incidence provides information on the electron momentum spectrum (EMS) of the local surface density of states (SDOS) *above* the surface. EMS and measurements of the Compton profile is a well-established technique for the bulk electronic structure employing photon-electron ($\gamma, \gamma e$) scattering,⁵ high-energy electron ($e, 2e$) scattering,⁶ and high-energy ion scattering.⁷ High collision energies are involved in order to assure that the momentum transfer in the collision Δk is large compared to the width of the momentum profile (of the order of the Fermi momentum k_F). Because of the large penetration depth at high energies these methods are not surface sensitive. For mapping out the SDOS above the surface only local nonpenetrating probes can be used which implies scattering with normal energy $E_{\perp} \leq 10$ eV. In turn, the energy for motion

parallel to the surface in grazing incidence is the projectile energy of a few keV here. The key point of the sensitivity to the Compton profile at such low energies is the existence of a so-called “classical velocity threshold” for KE, derived from a simple binary encounter model.⁸ For the occupied conduction band represented by a quasifree electron gas with Fermi velocity v_F (k_F in a.u.), Fermi energy E_F , and dispersion relation $E(k) = k^2/2$, the threshold projectile velocity for KE is given by

$$v_{th} = \frac{v_F}{2} [(1 + W/E_F)^{1/2} - 1], \quad (1)$$

where W is the work function. For $v_p < v_{th}$ the maximum momentum transferred to the electron $\sim 2(v_p + v_F)$ is insufficient to impart an energy on the electron necessary to overcome its binding energy W . This threshold behavior was consistent with experiments for grazing impacts of H and He atoms on Al(111).⁹ However, corrections to Eq. (1) are to be expected since the momentum distribution (Compton profile) of the local SDOS near the Fermi edge $\rho_s(\vec{k}, z, E_F)$ will, in general, contain high-momentum components $k > k_F$ due to the potential step near the surface, corrugation, and electronic correlations. Even a semi-infinite noninteracting jellium features high momentum components due to the (sharp) potential edge and broken translation symmetry along the surface. These high-momentum components are oriented along the surface normal (k_{\perp}) and ineffective for increasing the maximum energy transfer in collisions with a grazingly incident projectile moving parallel to the surface ($\vec{v}_p \parallel \vec{k}_{\parallel}$). In order to map out small contributions of off-shell high-momentum components ($k^2/2 \neq E$) parallel to the surface, large cross sections for binary electron-atom collisions are required. They should become most clearly visible in the subthreshold region [see Eq. (1)] when other on-shell processes are suppressed.

In our experiments we have scattered keV Ne and Ar atoms (Ne, Ar ion fractions below 10^{-5}) from an Al(111) surface under a grazing angle of incidence Φ_{in} of a few degrees where collisions with the solid proceed in the regime of surface channeling¹⁰ (reflection from topmost surface layer with defined trajectories). Since the distance of the closest approach is fairly large ($z_{min}=3$ a.u., as determined from rainbow scattering¹¹), modifications of the target surface are negligibly small. The large value of z_{min} also allows us to exclude promotion of occupied quasimolecular orbitals to vacuum in binary encounters between projectiles and target atoms as alternative mechanisms for ionization of projectiles which would require for the present systems $z_{min} \lesssim 1.5$ a.u.¹²

A key feature of the experimental setup is the coincident measurement of time-of-flight (TOF) spectra for projectiles scattered from the surface with the number of emitted electrons for each scattering event.¹³ From TOF spectra of neutralized beams, a significant contamination by metastables and thus electron emission by de-excitation of metastable atoms at surfaces (Penning ionization) can be excluded. Scattered projectiles are recorded 1.16 m behind the target by means of a channelplate electron multiplier. Electrons emitted from the surface are first collected via bias voltage of some 10 V applied to a highly transparent grid and then accelerated by +25 kV to the entrance of a surface barrier detector (SBD). SBD pulse heights are proportional to the electron number ejected per projectile.¹⁴ The clean atomically flat target surface is kept at a base pressure in the mid 10^{-11} mbar range and is prepared by cycles of grazing sputtering with 25 keV Ar⁺ ions and annealing at about 500 °C. The resulting surface roughness corresponds to a mean terrace width of about 1000 Å.¹⁵

For accurate measurements of γ near the threshold for KE [cf. Eq. (1)] one has to determine probabilities for the emission of zero (open circles) and one electron (full circles), shown in Fig. 1 for scattering of 3 keV Ne and 5 keV Ar atoms under $\Phi_{in}=2.2^\circ$. Solid curves in the figure result from a smoothing procedure for data without electron emission; dashed curves result from shifting these curves by a 5 eV energy loss which is much smaller than the mean energy loss itself. These shifted curves are intended to guide the eye for comparison with the minimum amount of energy transferred to a target electron necessary for electron emission [work function of Al(111) $W=4.3$ eV]. Soft collisions with small energy transfers to target electrons dominate the energy loss. Only a small subset of violent collisions result in energy transfers exceeding W .

Events with zero electrons are more probable by about a factor of 100 compared to emission of one electron (both spectra in Fig. 1 are shown in equal peak heights). Integration over the spectra for emission of zero and one electron (emission of more than one electron is negligible here) provides the probabilities for emission of i electrons; w_i with contributions from $i=0$ and $i=1$ only. The total electron yields

$$\gamma = \frac{\sum_{n=0}^{\infty} w_n n}{\sum_{n=0}^{\infty} w_n} = \frac{w_1}{w_0 + w_1}; \quad (2)$$

for the two data sets shown in Fig. 1 amount to $\gamma=0.004e^-/\text{atom}$ (3 keV Ne atoms) and $\gamma=0.014e^-/\text{atom}$

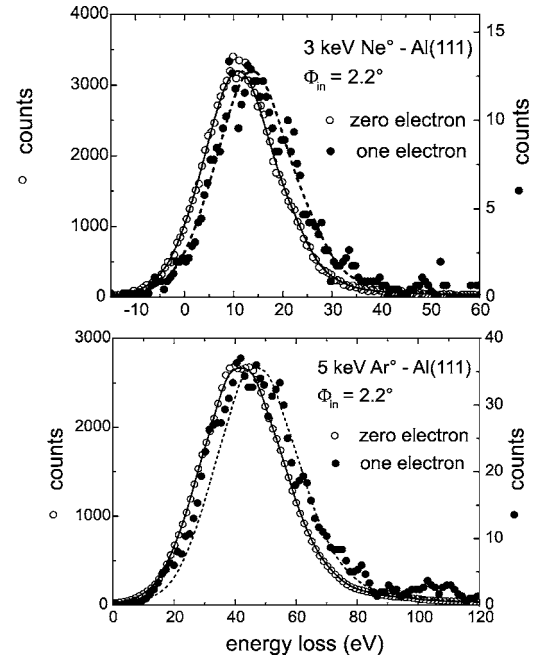


FIG. 1. Energy loss spectra for atoms scattered under a grazing angle of $\Phi_{in}=2.2^\circ$ at Al(111) coincident with emission of zero (open circles) and one electron (full circles). Scales are normalized to the same height at maximum. Solid curve; smoothed spline to data related to the emission of zero electrons; dashed curve, solid curve shifted by 5 eV; upper panel, 3 keV Ne atoms; lower panel, 5 keV Ar atoms.

(5 keV Ar atoms). The two data sets were recorded at projectile velocities $v_p=0.077$ a.u. (Ne) and $v_p=0.071$ a.u. (Ar) and thus *below* the threshold velocity $v_{th}=0.082$ a.u. calculated from Eq. (1) using the bulk Fermi velocity of Al. The key result of our studies is the observation of small but defined total electron yields for KE below v_{th} (see Fig. 2). Typical electron yields in the threshold region are smaller than the $\gamma \leq 0.05e^-/\text{atom}$ which is substantially larger than

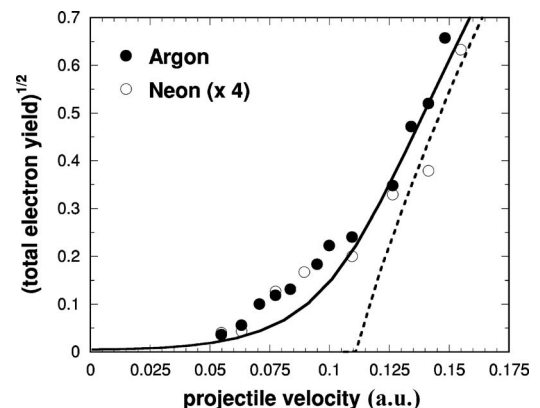


FIG. 2. Square root of total electron yields $\sqrt{\gamma_{KE}}$, as function of projectile velocity v_p for impact of Ne (open circles) and Ar (full circles) atoms on Al(111) under $\Phi_{in}=2.2^\circ$. Solid curve, present on-shell impulse approximations for subthreshold emission (see text) for Ar; dashed line is fit to data assuming the threshold law derived in Ref. 15. Note that data for absolute yields for Ne are multiplied by 4 (see text).

our detection limit for total electron yields of about 10^{-4} .

In order to elucidate the near-threshold behavior we have plotted in Fig. 2 $\gamma_{KE}^{1/2}$ as a function of projectile velocity for the impact of Ne and Ar atoms on Al(111) under $\Phi_{in}=2.2^\circ$. This plot is motivated by the threshold behavior $\gamma_{KE} \sim (v_p - v_{th})^2$ deduced from phase space arguments for a free electron metal and observed for light projectiles.¹⁶ Above v_{th} experimental data rapidly approach this behavior. Small but significant deviations are observed for $v_p \lesssim v_{th}$. Note that projectiles interact with electrons of the seldge in the region where the reduction of parallel momenta k_{\parallel} gives an enhancement of v_{th} compared to scattering within the bulk.

Our theoretical analysis invokes the on-shell approximation to the full impulse approximation.¹⁷ Accordingly,

$$\begin{aligned} & \frac{d^2\sigma}{dE d\Omega} \\ &= \frac{k'}{v_p} \int_{k_{min}}^{k_{max}} k dk \int_0^{2\pi} d\phi \sigma_{el}(q'^2/2, \cos \theta_e) \rho_s(\vec{k}, z_{min}, E_F). \end{aligned} \quad (3)$$

The approximative momentum distribution $\rho_s(\vec{k}, z_{min}, E_F)$ above the Al(111) surface at z_{min} and near the Fermi edge E_F was taken from Canney *et al.*¹⁸ with its distance dependence from the surface based on calculations with the ABINIT code.¹⁹ Bulk calculations show a sharp edge at the Fermi momentum $k_F=0.93$ a.u. in the $\langle 111 \rangle$ direction (along the surface normal) but tails towards higher electron momenta in $\langle 100 \rangle$ and $\langle 110 \rangle$ directions. The attenuation of high-momentum components of k_{\parallel} was calculated as a function of the distance z from the topmost atomic layer. High momentum components with $k > k_F=0.93$ a.u. persist for distances z as large as 5 a.u. The sharp edge for k_{\perp} is softened due to the breaking of translational symmetry at the surface.

In Eq. (3), θ_e denotes the polar angle of electron scattering relative to the direction of the incoming electron as seen in the rest frame of the atom, $\vec{q} = \vec{k} - \vec{v}_p$. In binary encounter approximation the on-shell approximation to the energy of the incoming electron is taken to be $E_e = q^2/2$, at which the elastic cross section is evaluated, that is, the initial binding is neglected. The final momentum in the projectile frame is denoted by \vec{q}' (with $\vec{q}'^2/2 = \vec{q}^2/2$) while the corresponding lab frame quantity is denoted by $\vec{k}' \cdot k_{min}$ and k_{max} denote the boundaries of the interval within which contributions of \vec{k} and scattering angles exist to yield a final state energy $E' = k'^2/2$ in the laboratory frame. The elastic cross section σ_{el} for scattering of conduction band electrons at noble gas atoms is calculated nonperturbatively by a partial-wave expansion²⁰ using atomic potentials derived from Hartree-Fock calculations.²¹ The strong interaction between the electron and the core of the projectile atom is thus taken into account to all orders. The surface potential enters the primary scattering process only via the initial-state momentum distribution. The interaction with the surface potential plays, however, an important role when multiple scattering in secondary collisions and transport of the liberated electron is considered. For energies relevant in the present context (electron

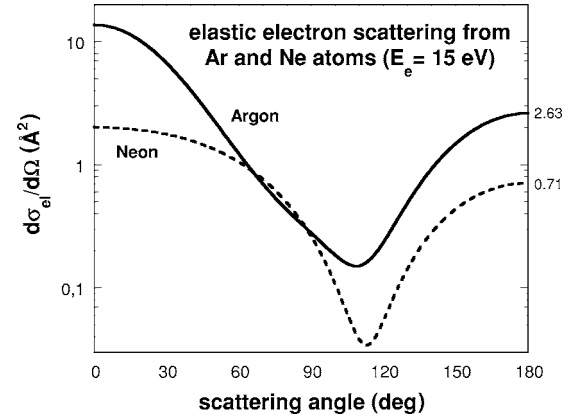


FIG. 3. Elastic cross sections for 15 eV electrons scattered off Ar and Ne atoms in gas phase calculated by partial-wave analysis using Hartree-Fock potentials [see Eq. (3)].

energy necessary to escape the target $E_{min} = E_F + W \approx 15$ eV) only very few partial waves contribute to σ_{el} leading to a single Ramsauer-Townsend minimum around 110° (see Fig. 3). Most remarkably, large-angle backscattering for noble gas atoms features a sizable cross section. The cross section rapidly increases with atomic number and is for Ar at backward angles ($\theta > 120^\circ$) a factor of 4 larger than for Ne and a factor 10–20 larger than for He.

The physics of subthreshold ionization by backscattering of high-momentum components built into Eq. (3) is schematically displayed in Fig. 4. As seen in the projectile rest frame, the initial momentum distribution is displaced by $-\vec{v}_p$. The prime candidates for KE reside in the shaded part of the initial momentum distribution [Fig. 4(a)]. After backscattering and transformation to the laboratory frame [Fig. 4(b)], electrons with final momentum k' larger than $k'_{min} = \sqrt{2(E_F + W)}$ (dashed circle) are energetic enough to be released into vacuum. Direct emission into vacuum at angles near $\pi/2$ is unlikely due to the small available phase space volume [Fig. 4(b)] and, more importantly, due to the suppression of elastic scattering near $\pi/2$ (see Fig. 3). The dominant

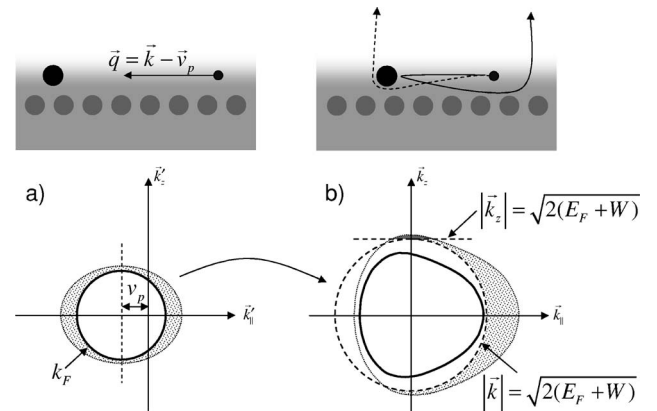


FIG. 4. Electron momentum distribution and backscattering, schematically. (a) (initial state prior to scattering), scattering geometry and momentum distribution in the projectile rest frame; (b) final momentum distribution in the laboratory (target) frame. Solid line, final states with initial momentum $k = k_F$.

contribution stems from backscattering ($\lesssim \pi$), where the cross section has a local maximum and a sizable phase space volume [shaded area in Fig. 4(b)]. These electrons will undergo additional (mostly elastic) scattering before escaping.

Due to the large transport mean free path of electrons in metals for energies $E_e < 20$ eV we assume an equal escape probability for all electrons with final momenta larger than $k' = \sqrt{2(E_F + W)}$. The total KE yield is then proportional to the phase space volume they occupy weighted with the cross section to be scattered there. The solid curve in Fig. 2 shows the subthreshold behavior of γ_{KE} for Ar projectiles normalized to the experimental data in the above-threshold region ($v_p \approx 0.125\text{--}0.15$ a.u.). Remarkably, results for Ne yield an almost identical velocity dependence with the absolute yield γ_{KE} a factor 4 smaller. The latter is an immediate consequence of the behavior of σ_{el} at backward angles (Fig. 3) and is in excellent agreement with the experimental data (see Fig. 2). We take this as strong evidence for the dominance of

backscattering at the origin of subthreshold KE.

In conclusion, we have presented measurements of electron emission at velocities of neutral rare gas projectiles below its classical threshold for kinetic emission.⁸ We explain the absence of a defined threshold by high-momentum components in the local spectral density of states above the surface. Large-angle scattering at the core of the neutral projectile, treated within an on-shell impulsive approximation, and transport out of the surface can account for the projectile velocity dependence of the total yield of emitted electrons γ_{KE} . The present results bear the potential to map out the momentum distribution near the Fermi edge and above the surface.

We thank the DFG, the AvH foundation (HPW), the FWF Austria, and EU (Contract No. HPRI-CT-2001-50036, CL and JB) for financial support.

*Author to whom correspondence should be addressed; Electronic address: winter@physik.hu-berlin.de

¹R. A. Baragiola, in *Low Energy Ion-Surface Interactions*, edited by J. W. Rabalais, (Wiley, New York, 1994).

²C. Lemell, J. Stöckl, J. Burgdörfer, G. Betz, H. P. Winter, and F. Aumayr, *Phys. Rev. Lett.* **81**, 1965 (1998).

³P. M. Echenique, R. M. Nieminen, and R. H. Ritchie, *Solid State Commun.* **37**, 779 (1981).

⁴J. I. Juaristi, M. Rösler, and F. J. Garcia de Abajo, *Phys. Rev. B* **58**, 15 838 (1998).

⁵C. Metz, Th. Tschentscher, P. Suortti, A. S. Kheifets, R. D. Lun, T. Sattler, J. R. Schneider, and F. Bell, *Phys. Rev. B* **59**, 10512 (1999).

⁶A. Kheifets, M. Vos, and E. Weigold, *Z. Phys. Chem.* **215**, 1323 (2001).

⁷F. Bell, H. Böckl, M. Wu, and H. Betz, *J. Phys. B* **16**, 187 (1983).

⁸R. A. Baragiola, E. V. Alonso, and A. Oliva Florio, *Phys. Rev. B* **19**, 121 (1979).

⁹S. Lederer, K. Maass, D. Blauth, H. Winter, HP. Winter, and F. Aumayr, *Phys. Rev. B* **67**, 121405(R) (2003).

¹⁰D. S. Gemmell, *Rev. Mod. Phys.* **46**, 129 (1974).

¹¹A. Schüller, G. Adamov, S. Wethekam, K. Maass, A. Mertens,

and H. Winter, *Phys. Rev. A* **69**, 050901(R) (2004).

¹²J. Lörincik and Z. Šroubek, *Nucl. Instrum. Methods Phys. Res. B* **164–165**, 633 (2000).

¹³A. Mertens, K. Maass, S. Lederer, H. Winter, H. Eder, J. Stöckl, HP. Winter, F. Aumayr, J. Vieffhaus, and U. Becker, *Nucl. Instrum. Methods Phys. Res. B* **182**, 23 (2001).

¹⁴F. Aumayr, G. Lakits, and H. P. Winter, *Appl. Surf. Sci.* **63**, 177 (1991).

¹⁵H. Winter, *Phys. Rep.* **367**, 387 (2002).

¹⁶H. Winter and HP. Winter, *Europhys. Lett.* **62**, 739 (2003).

¹⁷J. Wang, C. O. Reinhold, and J. Burgdörfer, *Phys. Rev. A* **44**, 7243 (1991).

¹⁸S. A. Canney, M. Vos, A. S. Kheifets, N. Clisby, I. E. McCarthy, and E. Weigold, *J. Phys.: Condens. Matter* **9**, 1931 (1997).

¹⁹X. Gonze, J. M. Beuken, R. Caracas, F. Detraux, M. Fuchs, G. M. Rignanese, L. Sindic, M. Verstraete, G. Zerah, F. Jollet, M. Torrent, A. Roy, M. Mikami, Ph. Ghosez, J.-Y. Raty, and D. C. Allanet, *Comput. Mater. Sci.* **25**, 478 (2002).

²⁰*The Theory of Atomic Collisions*, 3rd ed. (Clarendon Press, Oxford, 1965).

²¹R. H. Garvey, C. H. Jackman, and A. E. S. Green, *Phys. Rev. A* **12**, 1144 (1975).